Measurement of Arterial Input Functions for Dynamic Susceptibility Contrast Magnetic Resonance Imaging Using Echoplanar Images: Comparison of Physical Simulations with in Vivo Results

Guillaume Duhamel,[1] Gottfried Schlaug,[2] and David C. Alsop[1]*

Measurement of the arterial input bolus shape is essential to the quantification of mean transit time and blood flow with dynamic susceptibility contrast (DSC) MRI. Input functions derived from the echoplanar signal intensity within or near arteries are highly nonlinear, yet such input functions are widely used. We employed a physical model for the echoplanar signal intensity from an artery as a function of contrast agent concentration, artery size, and angle to the magnetic field to test approaches for the measurement of the arterial input function. The simulated results confirmed the strong nonlinearity of signal in the neighborhood of vessels. Of the input function measurement methods considered, the simulations suggested that measurement of signal near but not within a large vessel is most accurate, but mean transit times (MTT) calculated with these input functions are highly sensitive to peak bolus concentration. Input functions determined from voxels demonstrating the shortest first moment overestimated the MTT but the measured MTTs were more robust to changes in peak concentration. Characteristics of the measured in vivo input functions were consistent with the simulations. Our results emphasize the important contribution of input function errors to the uncertainty in MTT and blood flow imaging with DSC MRI.   Magn Reson Med 55:514–523, 2006. © 2006 Wiley-Liss, Inc.

Key words: blood flow; brain; dynamic susceptibility contrast; input function; mean transit time

Dynamic imaging of the brain as a bolus of intravascular contrast agent passes through the cerebral vasculature can, in principle, provide quantitative information on the blood flow and blood volume in brain tissue (1–4). While the technique was pioneered with X-ray computed tomography and iodinated tracers, it is now widely performed with the injection of magnetic susceptibility contrast agents and MRI. This dynamic susceptibility contrast (DSC) technique has been used extensively, especially for the characterization of ischemic stroke (5,6), and numerous reports of quantitative flow values obtained with this technique can be found in the literature (3,7,8). A large database of such studies in hyperacute stroke now exists in the stroke imaging community and accurate analysis of these data may lead to improved understanding of risk factors and potential treatments for acute stroke (9).

Cerebral blood flow is related to the broadening of the bolus as it passes through the microvasculature, so quantification of blood flow requires an accurate measure of the width of the bolus in the arteries before it enters the microvasculature. Input function widths are usually much wider than the broadening in the microvasculature of normal tissues. Hence, a small error in input function measurement can lead to a much greater error in the measured blood flow value. Absolute blood flow and blood volume measurement also requires knowledge of the absolute concentration, as well as the width, of the input function. Because absolute arterial concentration is difficult to measure and the relaxivity of contrast agents in the tissue microvasculature is not well calibrated, typically blood volume and flow are calculated in arbitrary units and values must be referenced to a control region elsewhere in the brain.

During the passage of a susceptibility contrast agent, the T_2- and T_2*- weighted signal intensity from arteries drops precipitously. Measurement of the arterial contrast concentration from the same images used to monitor the tissue signal intensity during the bolus passage would thus appear to be a straightforward process. However, a number of physical mechanisms can lead to severe nonlinearity and distortion of the R_2* and R_2 versus concentration curves. This has motivated several investigators to propose special sequences for input function measurement in large arteries at the base of the brain using signal intensity or phase (10,11). While these approaches are promising, the need for special sequences, and potentially reconstruction algorithms, has limited their application. These approaches also cannot permit the measurement of the input function very close to the brain region of interest (12,13) in order to avoid delay and dispersion effects (14).

Several groups have proposed input function measurement in standard T_2- or T_2*- weighted images using voxel selection criteria based on properties of the signal intensity curves, such as an early, large decrease in intensity (15), a large blood volume (16), a narrow full width at half maximum (FWHM) (3), anatomic location near but not within vessels (4,17), or clustering algorithms applied to time–intensity curves (12). Of these voxel selection approaches to input function measurement, none is based on a full understanding of the physical causes of nonlinearity

---

[1]Department of Radiology, Beth Israel Deaconess Medical Center, and Harvard Medical School, Boston, Massachusetts, USA.

[2]Department of Neurology, Beth Israel Deaconess Medical Center, and Harvard Medical School, Boston, Massachusetts, USA.

*Correspondence to: David Alsop, Department of Radiology/E/AN226, Beth Israel Deaconess Medical Center, 330 Brookline Avenue, Boston, MA 02215, USA. E-mail: dalsop@bidmc.harvard.edu
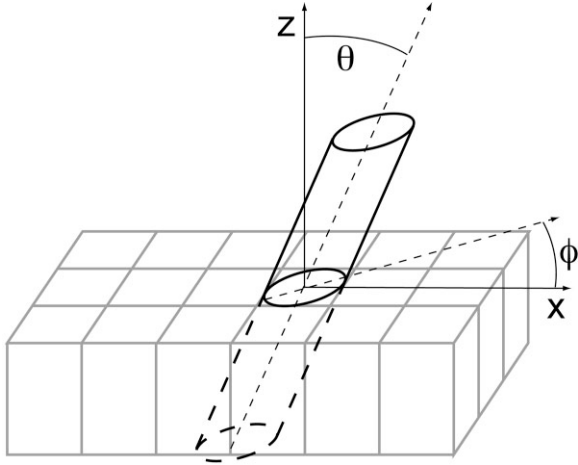
FIG. 1. The geometric model of a blood vessel passing through an imaged slice used for simulations. The blood vessel was approximated as an infinite cylinder at angles ϕ and θ relative to the *x*, frequency encoding, and *z*, main magnetic field direction, axes.

and only one has been compared to other measures of arterial concentration, albeit in a conference proceeding report (17). However, these approaches do potentially permit the analysis of DSC studies without the use of special sequences or approaches to input function measurement. Quantitative criteria, when supported by theoretical results, also permit the automatic determination of the input function, which can simplify and speed analysis in the clinical setting.

Here we report a theoretical study of the physical mechanisms responsible for relaxation nonlinearity in vessels and the implications of these mechanisms for the selection of voxels for input function determination in DSC studies employing echoplanar imaging. These theoretical results are then compared to signal intensity curves in DSC studies of six normal subjects and six patients presenting with acute stroke symptoms.

MATERIALS AND METHODS

Theoretical Model

In order to simulate the effect of contrast agent on echoplanar signal intensity, we created a geometric model of a vessel passing through an axial slice. The vessel was oriented at an angle θ to the main magnetic field and an angle ϕ to the phase direction as shown in Fig. 1. This geometric model was implemented on a two-dimensional grid with a grid size of 256 $\times$ 256 and a spacing equal to 100 μm. The eventual simulated images will have a spatial resolution of 1.88 mm and a field of view of 240 $\times$ 240 mm but the smaller region simulated on the grid spans only a smaller area of dimensions 25.6 $\times$ 25.6 mm corresponding to approximately 13 $\times$ 13 voxels. Averaging of the 2D grid across the slice direction was performed more efficiently in a later step, as described below. To simplify the analysis, it was assumed that the vessel was centered on a voxel and that the vessel was long enough that the magnetic fields it generated could be approximated by an infinite cylinder model. Because the combination of infinite

length, finite slice thickness, and finite field of view would lead to vessel signal within the slice extending to outside the field of view for θ values close to 90°, θ was constrained to less than 67.5°.

Signal intensities were calculated neglecting diffusion. Since only large vessels used as input functions are of interest, this approximation should be highly accurate. A T_2 and $T_2{}^*$ of 67 ms was assumed for the brain tissue surrounding the vessel. Other vessels were neglected in this analysis. Water diffusion effects around and into red blood cells in the vascular blood were included by the use of experimental measures of the $T_2{}^*$ of blood as a function of the paramagnetism of the blood plasma taken from the literature. Since the exchange time between red blood cells and plasma is much shorter than the 80–100 ms TEs typically used for spin echo DSC studies, T_2 was assumed equal to $T_2{}^*$. The $T_2{}^*$ was approximated by a quadratic fit to data reported by Akbudak et al. obtained from in vitro lamb blood at 1.5 T (18).

$$\frac{1}{T_2^*} = (5.18[Gd - DTPA(mM)]$$

$$+ 1.04[Gd - DTPA(mM)]^2 + 4.)s^{-1} \quad [1]$$

For normal hematocrits, the data were restricted to less than 7 mM Gd and consequently values of this equation for higher concentration may be an inaccurate extrapolation. For the TEs employed in this study, the attenuation is so great at higher concentrations that the vascular signal is essentially fully suppressed. Recent results in human blood (11) are consistent within this range and provide results for higher concentration. The magnetic effects of gadolinium in blood were based on the value for angular frequency shift, Ω, for Gd-DTPA in blood when in long tubes aligned with the main field direction (18).

$$\Omega = 2\pi(7.3s^{-1}mM^{-1})[Gd - DTPA] \quad [2]$$

This corresponds to a magnetic susceptibility of 3.4 $\times$ 10^{-7} mM^{-1} in MKS units, a value consistent with other sources (11,19).

In our model with vessels at arbitrary angles to the field and surrounding tissue, the frequency of signal from tissue and blood in the slice was calculated using a widely reported (20,21) analytical expression for the magnetic field as a function of distance from the center axis of the vessel.

For the blood, the frequency shift was given by

$$\omega_b = \frac{\Omega}{2}(2\cos^2\theta - \sin^2\theta) \quad [3]$$

and for the tissue

$$\omega_t = \frac{3\Omega\, r^2}{2\,\rho'^2}\sin^2\theta(\cos^2\phi' - \sin^2\phi')\,, \quad [4]$$

where *r* is the vessel radius, and ρ' and ϕ' are the cylindrical coordinates in the coordinate system where the vessel cylinder is aligned with the *z* axis and the magnetic field is in the *xz* plane. Since our simulation was per-

formed in a rectilinear coordinate system where the main magnetic field was oriented along the z axis, this tissue field expression was transformed to that coordinate system.

$$\omega_{outside}$$

$$= \frac{3\Omega}{2}r^2\sin^2\theta\frac{(((x\cos\phi + y\sin\phi)\cos\theta)^2 - (y\cos\phi - x\sin\phi)^2)}{(((x\cos\phi + y\sin\phi)\cos\theta)^2 + (y\cos\phi - x\sin\phi)^2)^2},$$

$$[5]$$

where x is the frequency direction and y is the phase direction.

The above magnetic field and relaxation time changes induced by the contrast agent have a great impact on echoplanar image intensity. These effects were simulated by calculating the phase and amplitude as a function of time at each grid point of our hyperresolved geometric model. To simplify and accelerate the calculations, frequency encoding was ignored in the calculations. Because frequency encoding is typically performed very rapidly and with very strong gradients, frequency shifts and relaxation have minimal impact on the point spread function in this direction. The signal at each echo time due to phase encoding gradients, frequency offsets, and T_2* was calculated by

$$S(k_m, y_j) = \sum_{i=1}^{255} S_0\exp$$

$$(- R_2(x_i, y_j)T_m)\exp(ik_m x_i)\exp(i\Phi(B(x_i, y_j)T_m)), \quad [6]$$

where k_m is the k space encoding corresponding to echo m, x and y are the coordinates in the 256×256 simulations grid (phase and frequency direction, respectively), R_2 is the signal relaxation, T_m is the time after excitation for echo m, and Φ is the phase shift at that time due to the field offset, $B(x, y)$. For the simulations, both a TE 50-ms gradient echo and a TE 100-ms spin echo acquisition were evaluated. The R_2 included the effects of contrast agent in the blood but neglected changes in the tissue R_2 due to contrast in the tissue microvasculature. The echo train duration was assumed to be 100 ms, comparable to the duration of a typical 128×128 acquisition, and 128 echoes were employed. The k steps were those corresponding to encoding of a 240×240 mm field of view. A slice thickness equal to 3.5 times the in-plane voxel resolution was used for all simulations. To account for the thickness of the slice, the complex signal as a function of position at each TE (the argument inside the summation in Eq. [6] was smoothed by convolution with a kernel three grid points wide and with length

$$l = \sec(\theta) \cdot slthick \quad [7]$$

and oriented along the projection of the cylinder axis onto the xy plane. Then the signal was totaled across the entire extent of the simulation in the phase direction and across the width of each voxel, 1.8 mm or eighteen 100-μm grid steps, in the frequency direction. After calculating the

signal for each of the echoes, a simulated image was reconstructed by Fourier transformation in the phase direction. The resulting image of the model, at a resolution identical to that of the echoplanar encoding, was then used for measuring the signal intensity response in the neighborhood of a vessel. All but the center 13×13 voxels of the simulated images contained little signal because of the limited spatial extent of the model grid and only signals from the 5×5 grid of voxels centered on the voxel containing the vessel were evaluated as candidate input functions because more distant voxels had small signal changes and were thus unlikely candidates for input function measurement locations.

Signal intensities were calculated for model vessels with 12 different angles between the tilt axis and the phase direction, ϕ, from 0 to 165° in uniform 15° steps, 20 different vessel radii, r, from 2.5 to 50% of the voxel width, and 15 different angles relative to the field direction, θ, from 1 to 67.5° in steps of 4.5°. Values of θ greater than 67.5° were removed because the vessel remains in-plane for more then the 13×13 voxel dimensions of the simulation. Simulations were performed for 20 approximately logarithmically spaced steps of blood Gd-DTPA concentrations from 0 to 20 mM.

Simulated Signal Responses to Bolus Passage

An assumed arterial concentration of the form

$$Input(t) = C(t - t_0)^n e^{-(t-t_0)/\tau} + A(1 - e^{-t/t_1}) \quad [8]$$

was defined, where t is time. The values $t_0 = 0$ s, $t_1 = 10$ s, $n = 2$, $\tau = 4$ s, and $A = 0.1\times C$ were selected and the peak concentration, C, was adjusted for different simulations. This input function does not include the small recirculation peak but otherwise represents the characteristics of a typical in vivo input concentration (10,11,16). The input function was sampled every 2 s over a total duration of 40 s.

Signal intensity curves for input functions of the above form were calculated by interpolation of the signal intensity versus concentration results from the theoretical model calculations above. Prior to interpolation, random noise at 2% of the voxel signal intensity was added to better simulate the noise level in experimental data. Ten different realizations of the random noise were performed for subsequent processing so that the propagation of noise through the analysis could be assessed. As is conventional for DSC studies, an apparent R_2* or R_2 curve was calculated from the logarithm of the signal intensity.

$$\Delta R_2^*(t) = -\frac{1}{TE}\ln\left(\frac{S(t)}{S(0)}\right) \quad [9]$$

After calculation, the R_2* curves were interpolated to 0.2 s resolution. These apparent R_2* curves were then considered for selection as sources of input function information.

Selection Criteria for Input Function Determination

Since many of the ΔR_2 curves are heavily distorted, our operational hypothesis was that some other criteria must

Table 1
Voxel Selection Criteria Evaluated on the Simulated R_2 Curves

Selection approach	Criteria	Threshold	Voxel selection
Volume	aCBV	-	100 max voxels
First moment	aCBV	>mincbv	
	FM		50, 100, or 500 max voxels
Model fit	aCBV	>mincbv	
	FM		2000 max voxels
	χ^2		10 min of FM voxels
Arterial phase	API		100 max voxels
Selection of vessel	Position in vessel		100 within vessel
Selection near vessel	Position near vessel		2 voxels from vessel

be applied besides location within a vessel to select voxels from which to determine an accurate input function. Based on the characteristics of the curves observed in the simulation, we first considered the combination of two criteria: a minimum threshold on the integral of the ΔR_2^* curve and then selection of some number of curves with the shortest first moment of the ΔR_2^* curve. These criteria remove voxels with only microscopic vessels, i.e., tissue, and those containing large veins, since venous contrast is delayed and broadened in a way that increases the first moment. Both the time integral, which is a measure of apparent cerebral blood volume for tissue (aCBV), and the first moment (FM) were calculated according to the formulae

$$aCBV = \sum_{k=0}^{T/\Delta t} \Delta R_2^* \Delta t \qquad FM = \frac{1}{aCBV}\sum_{k=0}^{T/\Delta t} \Delta R_2^*(k\Delta t)\Delta t , \quad [10]$$

where Δt is the interpolated temporal sampling of 0.2 s and T is the total time extent of the simulation, 40 s. Experience with these criteria suggested adding an additional criterion, the quality of a gamma variate fit to the ΔR_2^* curve. Candidate curves were fit to an expression of the form in Eq. [8] using a nonlinear least squares algorithm. The coefficient A in Eq. [8] was calculated from the mean of the last 10 points of the curve and the time t_1 for the rise of this constant term was fixed at 8 s because this term was poorly constrained by the fit. The remaining three terms, t_0, n, and τ, were initialized to values based on the aCBV, the FM, and the second moment of the curves. The χ^2 of the least squares fit was used as a measure of goodness of fit to the gamma variate model.

Two additional automatic selection criterion proposed by others were also evaluated. One criterion for voxel selection was early enhancement of apparent R_2 or R_2^* (15). This criterion is analogous to an "arterial phase" as employed in contrast angiography and does produce an excellent spatial map of the large arterial vessels in vivo. This criteria was implemented in the simulation by integrating the ΔR^* curves as in Eq. [10] except for a narrow range of T, from 0 to 2 s. A minimum threshold on the arterial phase integral (API) could then be applied to the simulated curves. A second, related criterion tested was a large blood volume, i.e., integrated ΔR_2^* over time (16). For the in vivo implementation, a weak threshold on arrival delay is necessary to eliminate venous voxels. This

was implemented in our simulation with a weak first moment threshold.

Finally we assessed anatomic criteria for selection. Both selection of the curve from a sample of voxels containing a larger vessel and selection from a voxel that was two voxels distant from the center of the vessel were evaluated. This approach was performed both for vessels at 1° to the field and at 67.5° to the field. Such selection is meant to approximate the placement of a voxel manually on in vivo data using anatomic knowledge of the position of vessels (17). We averaged 30 voxels for a random selection of ϕ and for r between 50 and 100% of the voxel width and for the two angles to the field.

For all but the anatomic criteria, we selected voxels from the entire range of simulation values. This implicitly assumes that in vivo, there is a random and relatively uniform distribution of vessel angles and radii. In such a distribution, the vessels are uniformly distributed in ϕ, but there are more vessels with θ further from 0°. To attempt to account for this, averages of input functions over selected vessels were weighted by $\sin\theta$. The voxel selection criteria evaluated on the simulations are summarized in Table 1.

A theoretical value for the aCBV expected in a gray matter voxel with true CBV of 7% was calculated using the static dephasing theory of Yablonskiy et al. (21) assuming a 50-ms TE gradient echo acquisition. This gray matter aCBV was used as a reference to define aCBV thresholds for input voxel selection from the simulations and also to provide an approximate connection to in vivo experimental data. The effect of the minimum CBV threshold on the results was assessed for values of 1.5, 3, 4.5, and 6 times aCBV of gray matter. For the spin echo acquisition, the gray matter aCBV expected was scaled by two thirds because the TE is twice as long but the spin echo relaxivity is approximately one third of the gradient echo relaxivity (22,23).

To provide a quantitative measure of the effect of imperfections in the derived input functions on the measurement of hemodynamic parameters, a simulation of the process of measuring mean transit time (MTT) was also performed. First, a simulated tissue concentration curve was generated. The initial assumed input function, Eq. [8], was numerically convolved with an exponential tissue response function of the form

$$R(t) = R_0 e^{-\frac{t}{MTT}} . \qquad [11]$$

The derived input functions were then used to measure the MTT by minimizing the least squares difference between the simulated tissue concentration curve and the convolution of the derived input function with a function of the form of Eq. [11] with both R_0 and MTT as free variables. This MTT "measurement" was then compared to the "true" value. MTT values from 2 to 20 s in 10 steps of 2s were evaluated. In addition, the MTT was calculated using the SVD deconvolution method of Ostergaard et al. (4) As in that work, a 20% SVD threshold was employed.

This approach was applied to both the gradient echo and the spin echo simulations. Gradient and spin echo simulations were tested with peak contrast agent concentration of 2.5, 5, 8, and 12 mM.

In Vivo Evaluation

Methods tested in the simulation were evaluated in in vivo data obtained from six normal adult male control subjects (between 25 and 40 years old) and six patients presenting with acute stroke within 13 h of symptom onset. The four female and two male stroke patients, mean age 75 years (SD 10), mean time imaged after symptom onset 5.0 h (SD 4), had significant hemodynamic abnormalities throughout much of the MCA distribution (four right, two left) and all had some diffusion changes supporting the diagnosis of acute stroke. All subjects were studied following a protocol approved by the local institutional review board and informed consent was obtained for all studies.

These data were obtained at 1.5 T using gradient echo echoplanar imaging with a field of view of 240 mm, a slice thickness of 7 mm, a matrix size of 128 × 128, and a TE of 50 ms. Forty successive images were acquired with a TR of 2 s in each of 12 slices. A bolus of Gd-DTPA (Magnevist, Schering, Berlin, Germany) at 0.1 mM/kg was administered followed by 20 cc of saline flush. A power injector was used for all but one of the clinical cases, for which manual injection was used.

Extracranial voxels were removed by intensity thresholding and the application of a morphometric erosion operator. Signal intensity versus time in each voxel was converted to apparent ΔR_2^* change as in Eq. [9]. The time of arrival of contrast in the vasculature was estimated by detecting the timepoint at which the average signal in the brain decreased by 10%. The integrated ΔR_2^* curve up to this timepoint was used for identifying arterial phase voxels. The relative blood volume was calculated from the integral of the entire ΔR_2^* curve and the first moment was calculated as in Eq. [10].

Candidate input functions were derived from voxels selected from the entire brain according to some of the criteria in Table 1. In vivo we employed a minimum blood volume cutoff of 2.25 times the average tissue blood volume. This approximated the 1.5 times the gray matter blood volume of the simulation without the need for segmentation of gray and white matter. The first moment threshold was varied to include only the shortest 50, 100, and 500 of the voxels. Gamma variate fitting is not reported in vivo because of noise issues in the simulations. The arterial phase criterion was also used to select the 100 voxels with the highest intensity on the arterial phase image. An approximation of the 2 voxels distant from the
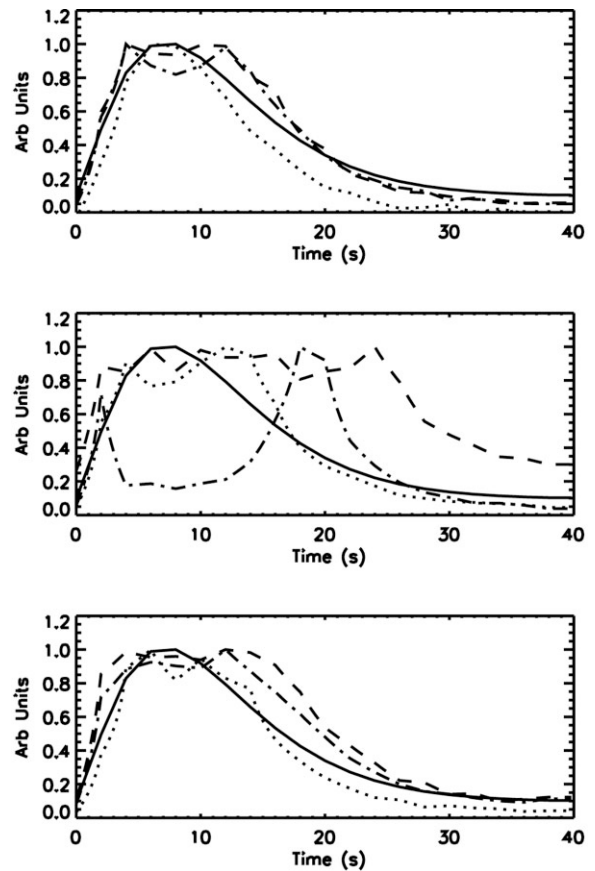

FIG. 2. Apparent R_2^* curves from nine randomly selected points with time integral greater than 1.5 times the estimated gray matter signal time integral. The normalized "true" input function is shown as a solid line. All curves were derived from the gradient echo simulations and a peak Gd concentration of 5 mM.

artery criterion used in the simulations was made by measuring the average of the signal 2 voxels anterior and posterior from each of the early arrival voxels. The 100 maximum blood volume points with first moment less than the average tissue first moment were used to calculate a blood volume criterion input function. The FWHM of the resulting input functions was calculated and used for quantitative comparison of input function width and variability.

RESULTS

Simulated signal response curves demonstrated a remarkable variability in shape and amplitude depending on position of the voxel and angle of the vessel (Fig. 2). Most of the curve shapes observed were broader than the original input function, although a subset of the curve shapes were narrower. The broader input functions tended to rise earlier than the true vessel concentration but then saturate. Typically, these broader functions were characterized by a low ratio of peak height to later, steady-state concentration level. The narrower input functions rose later than the true concentration but also returned more quickly. The narrow input functions had a low ratio of peak height to steady-state concentration level. Some input functions were vir-
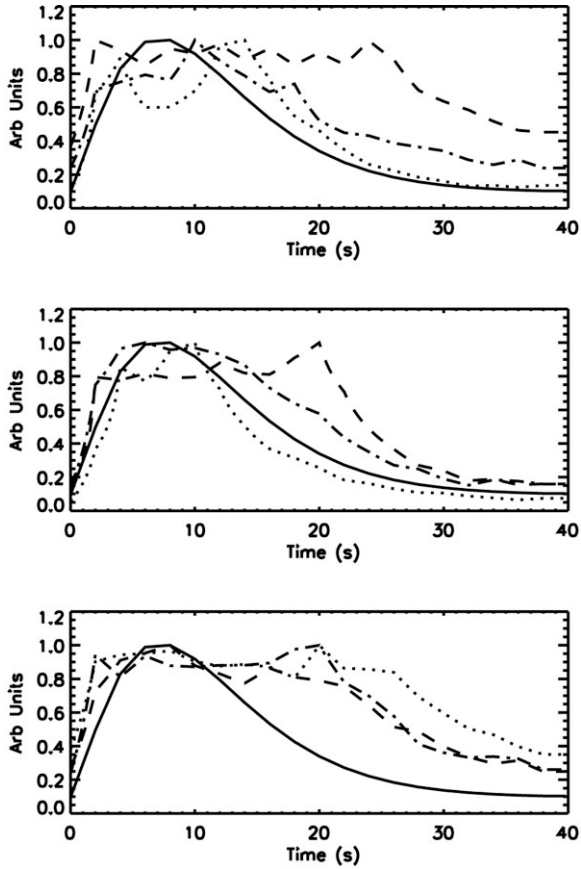
FIG. 3. Apparent *R*2 curves from nine randomly selected points with time integral greater than 1.5 times the estimated gray matter signal time integral. The normalized "true" input function is shown as a solid line. All curves were derived from the spin echo simulations and a peak Gd concentration of 8 mM.

FIG. 4. Simulated gradient echo, top, and spin echo, bottom, input functions. A peak gadolinium concentration of 5 mM for gradient echo and 8 mM for spin echo was assumed and a minimum CBV threshold equal to 1.5 times gray matter CBV and the 100 minimum first moment voxels were used for the first moment criterion.

tually identical in shape to the true vessel concentration. Similar types of behavior were also observed in the spin echo input functions (Fig. 3), although narrow input functions were less common.

Six different strategies were assessed for selecting input functions that approximate the shape of the true arterial input concentration. The simulation results were used to assess their performance (Fig. 4 and Table 2).

Of these approaches, several were clearly poor choices. Choosing voxels based on location within an artery produced very broad input functions that would be likely to lead to substantial errors in quantification. A related approach, the selection of voxels with large blood volume, produced similarly broad input functions. Both of these approaches suffered from the saturation phenomenon at higher concentrations that greatly broadens the input function. Input functions derived from the early arrival criterion often exhibited double peaks and were clearly distorted but somewhat less broad. Input functions derived based on the shortest first moment criterion tended to be narrower than the true input function. The two voxels from the vessel and gamma variate fit criteria provided the best approximation to the input function. Assessment of sum of square difference errors (Table 2) showed that the two voxel away criterion generally outperformed the other methods and the gamma variate fit criterion did almost as well for spin echo imaging but not gradient echo imaging.

Since the objective of the curve shape determination is to quantify MTT, the precision and accuracy of the MTT determination is an alternative criterion for assessing the input function measurement approaches. MTTs measured from the best least squares fit were only very weakly affected by the random noise added to the simulations (Table 3), with maximum errors for most of the input function measurement techniques comparable to the noise level of 2% or less. The gamma variate fit criterion was more
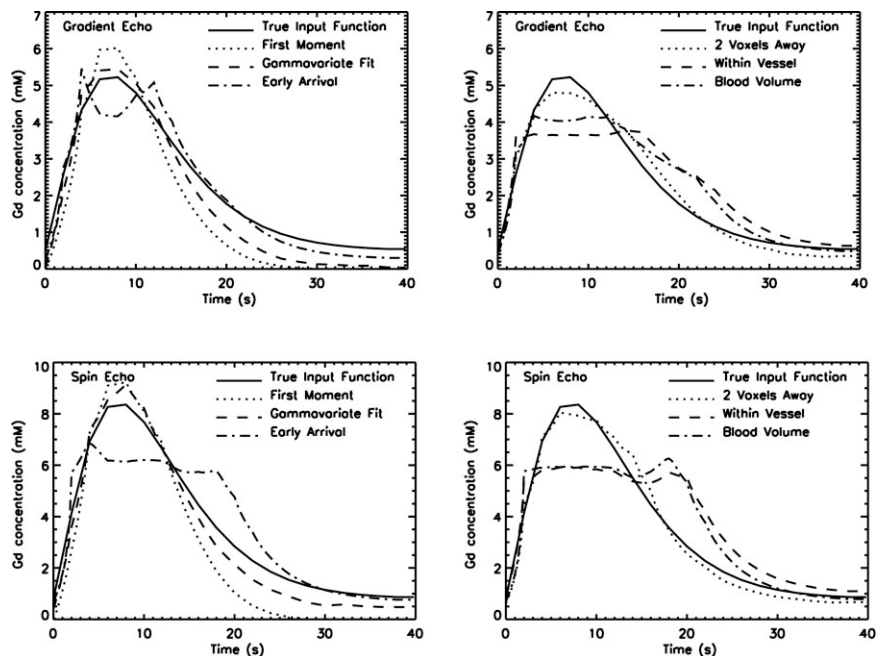
Table 2
Sum of Squares Error of Input Functions Derived from the Simulations Relative to the True Input Function for One Particular Peak Concentration and Totaled across Concentrations of 2.5, 5, 8, and 12 mM

Grad. echo	1.5× gm by threshold		3.0× gm by threshold		4.5× gm by threshold		6.0× gm by threshold	
	5 mm	Conc total	5 mm	Conc total	5 mm	Conc total	5 mm	Conc total
First mom 100	126.8	142.6	107.6	89.9	87	109.6	51.4	143.5
First mom 500	88.7	87.5	60.1	76.5	35.6	133.7	26.6	155.9
First mom 50	149.3	170	124.8	104.1	111.6	110.2	68.4	142.7
Gamma fit	51.4	50.72	31.9	89.4	13.2	162.2	11.4	135
Early arr	34.6	104.2	34.6	104.2	34.6	104.2	34.6	104.2
Blood vol	64.8	165.2	64.8	165.2	64.8	165.2	64.8	165.2
In vessel	123.1	206.6	123.1	206.6	123.1	206.6	123.1	206.6
2 vox away	12.5	28.4	12.5	28.4	12.5	28.4	12.5	28.4

Spin echo	1.5× gm by threshold		3.0× gm by threshold		4.5× gm by threshold		6.0× gm by threshold	
	8 mm	Conc total	8 mm	Conc total	8 mm	Conc total	8 mm	Conc total
First mom 100	146	135.8	103.2	106.4	51.4	65.6	20.8	50.8
First mom 500	82.7	86.4	36.9	45	10.8	31.4	22	60
First mom 50	151.1	151.5	126.5	118.1	73.7	82.1	33	62.5
Gamma fit	39.5	50.6	25.7	29.9	6.4	34.7	22.6	78.2
Early arr	209.3	185.2	209.3	185.2	209.3	185.2	209.3	185.2
Blood vol.	255.6	209.2	255.6	209.2	255.6	209.2	255.6	209.2
In vessel	248.4	197.1	248.4	197.1	248.4	197.1	248.4	197.1
2 vox away	32.7	40.7	32.7	40.7	32.7	40.7	32.7	40.7

sensitive to noise, especially for low blood volume thresholds with spin echo imaging. The average ratio of measured to true MTT was generally closest to unity for the two voxel away criterion. The gamma variate fit criterion was a close second. First moment criteria produced systematically higher MTTs while MTT from within the vessel, high blood volume, and early arrival criteria input functions tended to be systematically low. On the other hand, if precision, rather than accuracy, is most desirable, the SD of the MTT ratio was lowest for the first moment criteria, especially when a lower blood volume threshold was employed. For both the shortest first moment criterion and the two voxels away criterion, the ratio of measured to true MTT as a function of MTT is shown in Fig. 5 using all four different peak concentrations. The spread in MTT values is much smaller for the first moment criterion,

Table 3
Ratio of MTT Calculated by Least Squares Fitting from Derived Input Functions to True MTT Averaged across Peak Concentration and MTTs

Gradient echo	1.5× gm by threshold		3.0× gm by threshold		4.5× gm by threshold		6.0× gm by threshold	
	MTT rat	% SD	MTT rat	% SD	MTT rat	% SD	MTT rat	% SD
First mom 100	1.83 (0.4)	6	1.50 (0.5)	25.5	1.28 (0.5)	43.1	1.11 (0.9)	53.3
First mom 500	1.59 (0.2)	12.4	1.28 (0.2)	33.9	1.07 (0.3)	50.4	0.94 (1.0)	55.2
First mom 50	1.92 (0.6)	4.7	1.59 (0.7)	23.3	1.37 (0.7)	40.4	1.17 (1.2)	52.3
Gamma fit	1.35 (3.0)	17.5	1.12 (6.4)	41	0.92 (3.0)	49.3	0.83 (6.5)	49.2
Early arr	0.79 (1.2)	31.2	0.79 (1.2)	31.2	0.79 (1.2)	31.2	0.79 (1.2)	31.2
Blood vol	0.64 (0.8)	37	0.64 (0.8)	37	0.64 (0.8)	37	0.64 (0.8)	37
In vessel	0.59 (0.7)	44.5	0.59 (0.7)	44.5	0.59 (0.7)	44.5	0.59 (0.7)	44.5
2 vox away	0.94 (1.2)	23.3	0.94 (1.2)	23.3	0.94 (1.2)	23.3	0.94 (1.2)	23.3

Spin Echo	1.5× gm by threshold		3.0× gm by threshold		4.5× gm by threshold		6.0× gm by threshold	
	MTT rat	% SD	MTT rat	% SD	MTT rat	% SD	MTT rat	% SD
First mom 100	1.83 (0.6)	3.2	1.68 (0.7)	6.7	1.45 (0.5)	18.2	1.25 (0.6)	23.9
First mom 500	1.61 (0.3)	2.1	1.35 (0.3)	8.4	1.12 (0.3)	20.6	0.97 (0.3)	31.4
First mom 50	1.89 (0.8)	2.9	1.74 (1.1)	7	1.54 (0.8)	17.8	1.36 (0.8)	23.1
Gamma fit	1.32 (20.9)	2.4	1.05 (5.4)	15.9	0.95 (3.9)	25.2	0.88 (5.0)	35
Early arr	0.68 (1.0)	45.9	0.68 (1.0)	45.9	0.68 (1.0)	45.9	0.68 (1.0)	45.9
Blood vol	0.63 (0.7)	51	0.63 (0.7)	51	0.63 (0.7)	51	0.63 (0.7)	51
In vessel	0.59 (1.1)	40.8	0.59 (1.1)	40.8	0.59 (1.1)	40.8	0.59 (1.1)	40.8
2 vox away	0.91 (2.1)	23.4	0.91 (2.1)	23.4	0.91 (2.1)	23.4	0.91 (2.1)	23.4

Note. Average percentage standard deviation across 10 realizations of noise is shown in parentheses and SD is the percentage standard deviation across peak concentrations of 2.5, 5, 8, and 12 mM.

FIG. 5. Accuracy of the calculated MTT as a function of true MTT using input functions derived by the 100 shortest first moment (diamonds) and two voxels away from vessel (triangles) criteria. Points for each of the four peak concentrations, 2.5, 5, 8, and 12 mM, are shown. Gradient echo simulations and spin echo simulations using both a least squares fit and SVD methods for MTT determination are shown.
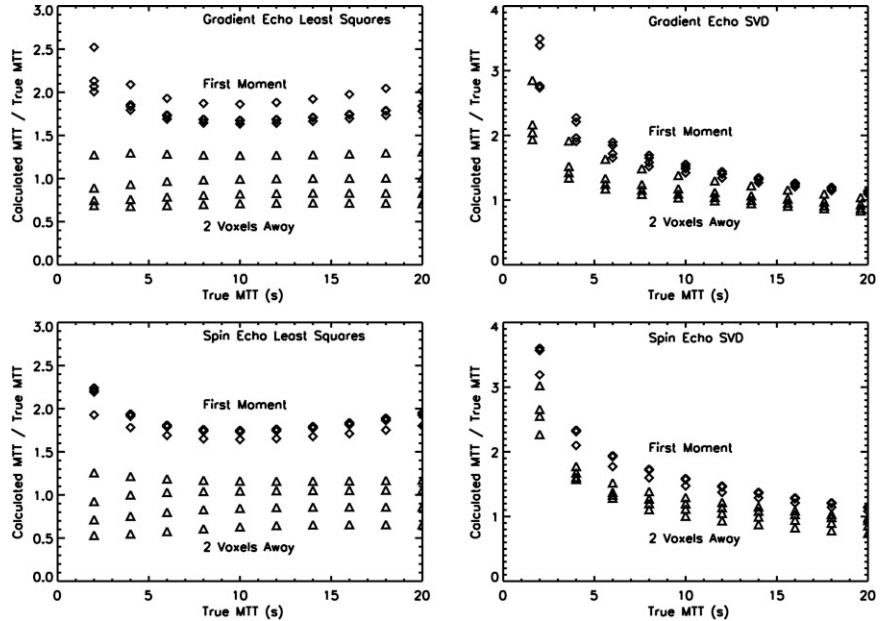
although the value of MTT is systematically high. When the singular value decomposition method was used to determine the MTT, the results were much more dependent on the true MTT. The sensitivity of the first moment criterion to peak concentration remained lowest and the MTTs measured were higher than with the two voxels away criterion. The ratio of measured to true MTT tended toward 1 for large MTTs but the MTT was overestimated by a large factor for low MTTs.

In vivo input functions determined using similar criteria to those used in the simulations showed similar qualitative behavior (Table 4). The FWHM of the first moment criterion was the narrowest, the largest blood volume had the highest FWHM, and the two voxels away criterion was intermediate. The FWHM of the blood volume criterion was actually higher than the tissue response and the early arrival criterion was almost equal in FWHM to that of the tissue response. The SD of the difference between left and right hemisphere input functions was small, less than 3% for all the methods, with the first moment criterion having the highest variability. On the other hand, the SD of the FWHM across the normal volunteers was lowest for the first moment criterion. Example input functions from one volunteer are shown in Fig. 6.

Measured input functions in the acute stroke patients were broader than in the volunteers and were also nonsignificantly broader in the affected hemisphere than in the contralateral hemisphere. The same qualitative ordering of the FWHM of the input functions was observed in the patients. Sample input functions from the affected and unaffected hemisphere of one patient are shown in Fig. 7.

DISCUSSION

Measurement of the shape of the arterial input function is essential to quantification of MTT and consequently cerebral blood flow using the DSC technique. For more than a decade, the signal intensity from or near a major artery has been employed for the purpose of quantification without theoretical justification and with minimal validation. Al-

Table 4
Full Width at Half Maximum of the Derived in Vivo Input Functions for Six Patients and Six Controls

Controls	In vessel	2 vox away	Blood vol	FM 50	FM 100	FM 500	Tissue
Whole brain	9.13 (1.48)	8.69 (0.73)	10.75 (0.79)	7.82 (0.53)	8.11 (0.38)	8.63 (0.55)	9.33 (0.81)
Left	9.02 (1.23)	8.72 (0.71)	10.26 (0.70)	8.24 (0.36)	8.4 (0.31)	9.00 (0.55)	9.33 (0.75)
Right	9.06 (1.27)	8.60 (0.69)	10.62 (0.57)	7.75 (0.79)	8.22 (0.56)	8.89 (0.77)	9.32 (0.87)
Right–left SD	0.24	0.11	0.19	0.7	0.34	0.3	0.14

Patients	In vessel	2 vox away	Blood vol	FM 50	FM 100	FM 500	Tissue
Whole brain	14.04 (5.29)	13.11 (5.43)	16.3 (4.66)	11.75 (4.03)	11.72 (4.26)	12.48 (4.87)	15.83 (6.60)
Contralateral	15.72 (8.28)	13.07 (5.44)	14.58 (4.79)	11.30 (4.17)	11.53 (4.3)	12.55 (5.07)	14.22 (5.90)
Ipsilateral	15.74 (7.96)	13.27 (4.81)	16.48 (5.11)	11.86 (4.21)	12.08 (4.16)	13.5 (5.00)	16.77 (6.63)
Ipsi contra p	0.98	0.67	0.005	0.22	0.17	0.014	0.016

Note. All FWHM are in seconds. Right–left SD is the standard deviation across normal subjects of the difference in FWHM determined only from the right and left sides. Ipsi contr is the two-tailed paired Student *t* test probability of the difference in FWHM between input functions determined from the side ipsilateral to the stroke-related hemodynamic abnormality and the side contralateral. Tissue is the FWHM of the average signal across the brain or hemisphere.
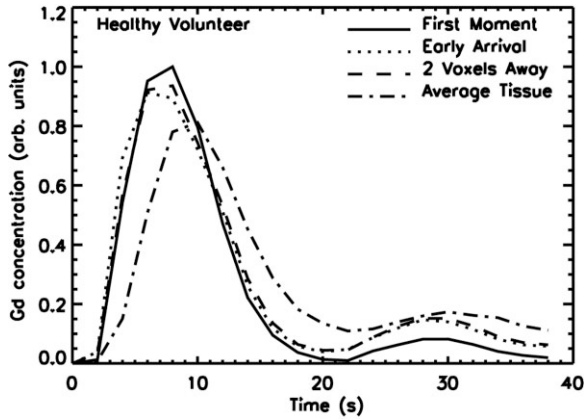
FIG. 6.   Input functions derived from a healthy volunteer. Curves derived from the 100 shortest first moment, two voxels away, and early arrival criteria are shown. The average tissue curve is also shown for comparison.

though several investigators have emphasized the problems with input function measurement and developed new approaches to input function measurement using special acquisition and processing strategies (10,11,13), the acquisition of a simple series of echoplanar images during bolus passage has become widely used. A large body of acquired data in important diseases such as acute stroke now exists and clinical prediction strategies have been based on this experience. This investigation was intended to determine the best strategy for measuring an input function from such data and to assess the remaining systematic errors when using this approach.

Our simulations based on a physical model emphasized the strong nonlinearity of input functions derived from voxels near large arteries. Such nonlinearity complicates the measurement of accurate input functions based on anatomic criteria alone. The simulations were used to select criteria for identifying undistorted curves based on characteristics of their shape, amplitude, and location. This approach was modestly successful at producing good curves and accurate MTT values but significant sources of error remain. In addition, the simulations are an imperfect model of the actual physical problem. The simulations did not include vessels at angles greater than 67.5° to the main field or vessels not centered within a voxel and did not consider the effects of vessel curvature or the signal changes due to the blood volume and flow of the tissue in the voxel. Nevertheless, the results provide guidance as to the behavior of signal nonlinearities, their potential cor-

ruption of quantification approaches, and possible approaches to minimizing their impact.

A number of strategies for identifying voxels for input function measurement have been suggested. A widely used criterion of selecting a voxel near a major artery (4,17) appears to be moderately accurate for gradient and spin echo imaging. Automatic criteria for selecting input functions are desirable and several have been proposed (15,16). While our first moment and gamma variate fit criteria are qualitatively similar to one of the first suggested approaches (3), other automatic approaches based on blood volume (16) or early arrival (15) would appear to be undesirable. Classification of input voxels based on clustering criteria (12) or independent component analysis (24) have been proposed but these methods lack a simple method for comparison with theory.

The shape of the arterial function can vary with injection method and volume and also with subject cardiovascular physiology. The purpose of measuring the arterial input function is to control for variations in bolus parameters. While, in principle, absolute blood volume and flow can be measured, calibration challenges due to differences in tissue and vascular relaxation make such absolute quantification difficult. Absolute quantification of MTT, on the other hand, depends only on the bolus shape and should be feasible. Our simulations can be used to assess the impact of bolus changes on measured MTT. For most input function measurement criteria, the measured MTT is highly sensitive to the peak bolus concentration. The effect of changes in bolus width, with constant peak concentration, can be assessed by scaling the time coordinate in the simulations. Doubling the bolus width is analogous to multiplying the MTT in the simulations by a factor of 2. For the least squares fit measurement method, the measured MTT is quite linear in the true MTT and the bolus broadening does not produce systematic error. When the SVD measurement method is employed, changes in bolus width have a strong effect on the measured MTT. If precision in the presence of changes in bolus width and peak concentration is highly desirable, our simulations suggest that the shortest first moment criterion is best, despite the systematic overestimation of MTT.

In addition to the problem of accurate global input function determination, there is increasing interest in measuring a local input function to eliminate delay and especially dispersion of the input function in transit to the tissue. While the partial success at determining input functions purely with curve shape criterion suggests that extension to local input functions may be possible, the increased
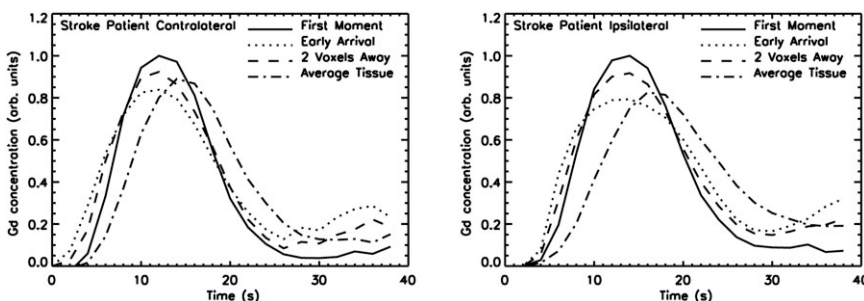

FIG. 7.   Input functions derived from a patient presenting with acute middle cerebral artery stroke. Curves derived from the 100 shortest first moment, two voxels away, and early arrival criteria are shown. The average tissue curve is also shown for comparison. Curves obtained from the side contralateral to the abnormality, left, and ipsilateral to the abnormality, right, were separately calculated.

errors associated with determining input functions with only a few vessels is a matter for concern. The higher FWHM in the ipsilateral hemisphere of our stroke patients is a crude illustration of how local input functions with certain criteria may help reduce dispersion effects in DSC quantification.

Imperfect input function measurement is only one of several inaccuracies in DSC imaging, including delay and dispersion of the arterial bolus (14), uncertainties in tissue relaxivity (25), and large vessel contamination (26), that compromise its accuracy. The importance of hemodynamic information in combination with other types of contrast provided by MRI, however, make DSC a useful tool in a number of pathologies. Our results suggest some approaches to obtaining an approximate input function. They also emphasize the imperfect removal of input bolus shape effects on the calculated MTT, especially peak height. Minimizing the variability in shape and peak height of the bolus is highly desirable for precise, if not perfectly accurate, MTT and blood flow measurement.

REFERENCES

1. Axel L. Cerebral blood flow determination by rapid-sequence computed tomography: theoretical analysis. Radiology 1980;137:679–686.
2. Rosen BR, Belliveau JW, Buchbinder BR, McKinstry RC, Porkka LM, Kennedy DN, Neuder MS, Fisel CR, Aronen HJ, Kwong KK, et al. Contrast agents and cerebral hemodynamics. Magn Reson Med 1991; 19:285–292.
3. Rempp KA, Brix G, Wenz F, Becker CR, Guckel F, Lorenz WJ. Quantification of regional cerebral blood flow and volume with dynamic susceptibility contrast-enhanced MR imaging. Radiology 1994;193: 637–641.
4. Ostergaard L, Weisskoff RM, Chesler DA, Gyldensted C, Rosen BR. High resolution measurement of cerebral blood flow using intravascular tracer bolus passages. Part I: Mathematical approach and statistical analysis. Magn Reson Med 1996;36:715–725.
5. Schlaug G, Benfield A, Baird AE, Siewert B, Lovblad KO, Parker RA, Edelman RR, Warach S. The ischemic penumbra: operationally defined by diffusion and perfusion MRI. Neurology 1999;53:1528–1537.
6. Sorensen AG, Copen WA, Ostergaard L, Buonanno FS, Gonzalez RG, Rordorf G, Rosen BR, Schwamm LH, Weisskoff RM, Koroshetz WJ. Hyperacute stroke: simultaneous measurement of relative cerebral blood volume, relative cerebral blood flow, and mean tissue transit time. Radiology 1999;210:519–527.
7. Ostergaard L, Smith DF, Vestergaard-Poulsen P, Hansen SB, Gee AD, Gjedde A, Gyldensted C. Absolute cerebral blood flow and blood volume measured by magnetic resonance imaging bolus tracking: comparison with positron emission tomography values. J Cereb Blood Flow Metab 1998;18:425–432.
8. Lin W, Lee JM, Lee YZ, Vo KD, Pilgram T, Hsu CY. Temporal relationship between apparent diffusion coefficient and absolute measurements of cerebral blood flow in acute stroke patients. Stroke 2003;34: 64–70.
9. Latchaw RE, Yonas H, Hunter GJ, Yuh WT, Ueda T, Sorensen AG, Sunshine JL, Biller J, Wechsler L, Higashida R, Hademenos G. Guidelines and recommendations for perfusion imaging in cerebral ischemia: A scientific statement for healthcare professionals by the writing group on perfusion imaging, from the Council on Cardiovascular Radiology of the American Heart Association. Stroke 2003;34:1084–1104.
10. Akbudak E, Conturo TE. Arterial input functions from MR phase imaging. Magn Reson Med 1996;36:809–815.
11. van Osch MJ, Vonken EJ, Viergever MA, van der Grond J, Bakker CJ. Measuring the arterial input function with gradient echo sequences. Magn Reson Med 2003;49:1067–1076.
12. Rausch M, Scheffler K, Rudin M, Radu EW. Analysis of input functions from different arterial branches with gamma variate functions and cluster analysis for quantitative blood volume measurements. Magn Reson Imaging 2000;18:1235–1243.
13. Alsop DC, Wedmid A, Schlaug G. Defining a local input function for perfusion quantification with bolus contrast MRI. In: Proceedings of the 10th Annual Meeting of ISMRM, Honolulu, Hawaii, USA, 2002. p 659.
14. Calamante F, Gadian DG, Connelly A. Delay and dispersion effects in dynamic susceptibility contrast MRI: simulations using singular value decomposition. Magn Reson Med 2000;44:466–473.
15. Smith AM, Grandin CB, Duprez T, Mataigne F, Cosnard G. Whole brain quantitative CBF and CBV measurements using MRI bolus tracking: comparison of methodologies. Magn Reson Med 2000;43:559–564.
16. Carroll TJ, Rowley HA, Haughton VM. Automatic calculation of the arterial input function for cerebral perfusion imaging with MR imaging. Radiology 2003;227:593–600.
17. Porkka L, Neuder M, Hunter G, Weisskoff RM, Belliveau JW, Rosen BR. Arterial input function measurement with MRI. In: Proceedings of the 10th Annual Meeting of SMRM, San Francisco, CA, USA, 1991. p 120.
18. Akbudak E, Hsu RM, Conturo TE. ΔR^* and $\Delta \Phi$ contrast agent perfusion effects in blood: quantification and linearity assessment. In: Proceedings of the 6th Annual Meeting of ISMRM, Sydney, Australia, 1998. p 1197.
19. Weisskoff RM, Kiihne S. MRI susceptometry: image-based measurement of absolute susceptibility of MR contrast agents and human blood. Magn Reson Med 1992;24:375–383.
20. Albert MS, Huang W, Lee JH, Patlak CS, Springer CS, Jr. Susceptibility changes following bolus injections. Magn Reson Med 1993;29:700–708.
21. Yablonskiy DA, Haacke EM. Theory of NMR signal behavior in magnetically inhomogeneous tissues: the static dephasing regime. Magn Reson Med 1994;32:749–763.
22. Simonsen CZ, Ostergaard L, Smith DF, Vestergaard-Poulsen P, Gyldensted C. Comparison of gradient- and spin-echo imaging: CBF, CBV, and MTT measurements by bolus tracking. J Magn Reson Imaging 2000;12:411–416.
23. Marstrand JR, Rostrup E, Rosenbaum S, Garde E, Larsson HB. Cerebral hemodynamic changes measured by gradient-echo or spin-echo bolus tracking and its correlation to changes in ICA blood flow measured by phase-mapping MRI. J Magn Reson Imaging 2001;14:391–400.
24. Calamante F, Morup M, Hansen LK. Defining a local arterial input function for perfusion MRI using independent component analysis. Magn Reson Med 2004;52:789–797.
25. Kiselev VG. On the theoretical basis of perfusion measurements by dynamic susceptibility contrast MRI. Magn Reson Med 2001;46:1113–1122.
26. Carroll TJ, Haughton VM, Rowley HA, Cordes D. Confounding effect of large vessels on MR perfusion images analyzed with independent component analysis. Am J Neuroradiol 2002;23:1007–1012.